A Solution to the Parameter Selection and Current Static Error Issues with Frequency Shift Islanding Detection Methods

Menghua Liu[1], Wei Zhao[1*], Qing Wang[2], *Senior Member, IEEE*, Songling Huang[1], *Senior Member, IEEE*, and Kunpeng Shi[1]

Abstract— **Frequency shift islanding detection methods have been widely used in inverter-based distributed generations. Two representatives of such methods, Sandia frequency shift (SFS) and reactive current perturbation (RCP) methods, are investigated in this paper. The investigation reveals two main issues with these two methods, i.e., parameter selection scheme for positive feedback gain and current static error. The current parameter selection scheme, in particular, is considered unreliable and inconvenient in this paper, for it has not considered the weakening effect of PI regulators on positive feedback and the positive feedback gain is actually obtained by trial and error, which makes it difficult to use such methods well in field environments. In view of these issues, this paper proposes a solution that contains an improved method to eliminate current static error and a reliable and convenient parameter selection scheme based on system stability analyses. The final simulations and experiments verify the good performance of the improved method and the parameter selection scheme.**

***Index Terms*—current static error, Instability, Islanding detection, parameter selection, perturbation to the rate of change of reactive current**

I. INTRODUCTION

WITH the development of inverter-based distributed generation (DG), the relevant measurement and control technology has achieved great progress. As a fault diagnosis function, islanding detection is indispensable in DG and has attracted more and more attention. Various islanding detection methods have been proposed. In general, these methods are categorized as remote methods and local methods, the latter of which are divided into passive methods and active methods. As active methods have a smaller non-detection zone (NDZ) as well as advantages in cost, they have been the mainstream methods. This paper will discuss frequency shift islanding detection methods, which are a major type of active method.

Active methods perturb the output currents or voltages of DG units, and judge an island event according to the resultant responses afterwards. As for frequency shift methods, two common ones were Sandia frequency shift (SFS) and slip-mode frequency shift (SMS) methods, which were aimed at perturbing the output current phases of inverters [1], [2]. By comparison, [3]–[7] perturbed reactive currents. [5] indicated that such methods could decouple the current control, which partially solved the problems with SFS and SMS methods, while [7] revealed a critical problem that SFS and SMS methods could not be used under non-unity power factor (non-UPF) control. [8]–[10] perturbed reactive power, which was similar to perturbing reactive currents in principle. [11] and [12] concentrated on the parameter selection issue with the SFS method to reduce NDZ. [13] improved the perturbation mode of the SMS method to mitigate the effect on current. [14] proposed a new parameter design criterion for the SFS method, which improved the conventional design criteria to a certain extent.

Apart from this, other types of islanding detection methods have also attracted many studies. As current injection methods, [15] and [16] monitored the changes of voltage and network impedance, respectively, which were used as the indices for islanding detection. [17] pointed out a misjudgment problem with the irregular current injection methods and proposed a solution. [18] and [19] belonged to the passive methods, which measured the network impedance passively and employed the wavelet theory, respectively. It was noteworthy that due to the maturity of the theory of signal processing and artificial intelligence and widespread use in other fields, substantial passive methods employing them were emerging [20]–[22]. [23] was a remote method, which judged island events by means of the data collected by phasor measurement units. Recently, islanding detection in DC-grid was studied, although it seemed that the islanding detection was simpler in DC-grid than in AC-grid [24], [25]. Moreover, some hybrid approaches that integrated multiple different methods were also studied [1], [26], [27]. Such hybrid approaches were indeed more dependable, despite the complexity.

Although frequency shift methods have been improved from various angles, two issues, i.e., parameter selection and current static error, still need to be further studied.

Firstly, the existing parameter selection scheme is unreliable and inconvenient. The perturbations from these methods were generally integrated into the control loops. The influence of the generation control on the perturbations was usually overlooked

Correspondence to: Prof. W. Zhao.
[1]State Key of Power Systems, Department of Electrical Engineering, Tsinghua University, Beijing, 100084, China
[2]Department of Engineering, Durham University, Durham, DH1 3LE, United Kingdom

before, while in fact the control system would treat the perturbations as interference and suppress them, which would weaken the perturbation effect undoubtedly. Therefore the derived selection schemes for the positive feedback gain, which was related to the perturbation, were unreliable. The existing selection schemes determined a minimum rather than a proper value for the positive feedback gain, and [28] indicated that the positive feedback gain should be restricted for the power system stability. Consequently, a moderate positive feedback gain could only be obtained via a trial and error procedure, whose simple flow chart is shown in Fig. 1. As a parameter selection scheme, this trial and error was very inconvenient in applications.

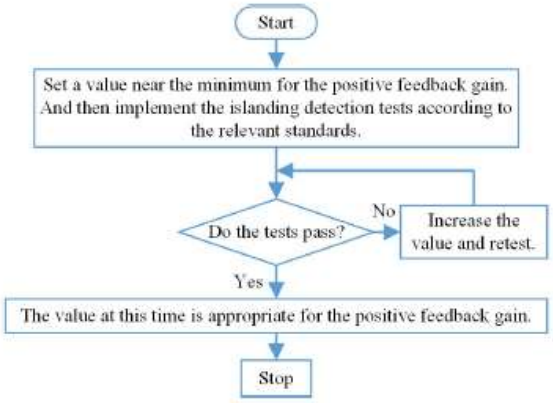

Fig. 1. A simple trial and error procedure

Furthermore, the existing frequency shift methods will result in current static errors, which were not valued in literature. Although these static errors were small, they indeed degraded the quality of current control.

In view of the above problems, this paper proposes a reliable and convenient parameter selection scheme and an improved frequency shift method, which can generally eliminate the current static errors. Even though [11] also addressed the mentioned parameter selection issue, it will be seen that the scheme proposed in this paper is much easier to realize, for it requires less software and hardware and can even run on a host computer.

This paper is organized as follows. Section II introduces two representative frequency shift methods and reveals their problems. Then section III proposes an improved islanding detection method and a parameter selection scheme. Sections IV and V test and validate the previous analyses by simulations and experiments, respectively. Finally, a conclusion is drawn.

II. Two Representative Frequency Shift Islanding Detection Methods and Their Problems

Some early literature has revealed that a parallel *R, L, C* load model is more likely to cause a failed islanding detection [29], [30]. IEEE Std 1547.1-2005 has used such a load as the test model [31]. Thus, it is the default load in this paper. A general DG diagram is shown in Fig. 2. As classic inverter-based frequency shift methods, the SFS and reactive current perturbation (RCP) methods are chosen as the representatives to be analyzed in this paper.

A. SFS Method and Its Problems

1) Principle Introduction: As shown in Fig. 2, (1) is true in an island condition (i.e., S_g tripped off).

$$\begin{cases} P_{\text{inv}} = P_{\text{load}} = 3U^2/(2R) \\ Q_{\text{inv}} = Q_{\text{load}} = 3U^2[1/(2\pi f_{\text{act}}L) - 2\pi f_{\text{act}}C]/2 \end{cases} \quad (1)$$

where P_{inv} and Q_{inv} are the output active power and reactive power of the inverter, respectively; P_{load} and Q_{load} are the load active power and reactive power, respectively; *R, L* and *C* represent the load; and U and f_{act} are the actual voltage amplitude and frequency at the point of common coupling (PCC), respectively.

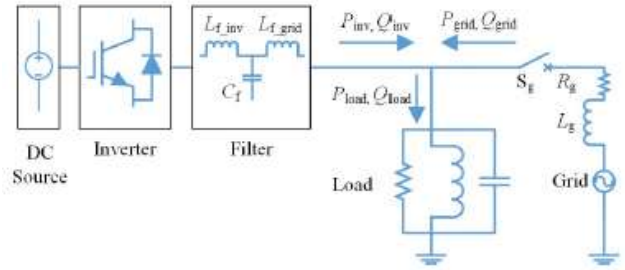

Fig. 2. Inverter-based DG

From (1) and the definitions of load quality factor Q_f and resonant frequency f_0 shown in (2), (3) can be derived.

$$\begin{cases} Q_{\text{f}} = R\sqrt{C/L} \\ f_0 = 1/(2\pi\sqrt{LC}) \end{cases} \quad (2)$$

$$f_{\text{act}} = f_0(\sqrt{4Q_{\text{f}}{}^2P_{\text{inv}}{}^2 + Q_{\text{inv}}{}^2} - Q_{\text{inv}})/(2Q_{\text{f}}P_{\text{inv}}) \quad (3)$$

According to the relationship shown in (4), where θ_{inv} is the angle by which the output current of the inverter leads the PCC voltage, f_{act} can also be represented as (5).

$$\tan\theta_{\text{inv}} = -Q_{\text{inv}}/P_{\text{inv}} \quad (4)$$

$$f_{\text{act}} = f_0(\sqrt{4Q_{\text{f}}{}^2 + \tan^2\theta_{\text{inv}}} + \tan\theta_{\text{inv}})/(2Q_{\text{f}}) \quad (5)$$

Equation (5) shows that the perturbation to θ_{inv} can lead to a deviation of f_{act}. The SFS methods are just based on this, whose implementation schemes are shown in Fig. 3, where there is the equation below according to the decoupling control scheme mentioned in [32].

$$L_{\text{f}} = L_{\text{f\_inv}} + L_{\text{f\_grid}}$$

θ_f represents the perturbation angle and is set as (6) [32], [33].

$$\theta_{\text{f}} = [cf_0 + k_{\text{SFS}}(f - f_{\text{g}})]\pi/2 \quad (6)$$

where cf_0 is an initial chopping fraction; k_{SFS} is a positive feedback gain; f_g is the nominal frequency of a grid; and f is the frequency measured by a phase-locked loop (PLL).

2) Problems with the SFS Method: Although the SFS method has proven to be very efficient for islanding detection, the four problems below still exist [34].

a) There is currently no reliable and convenient selection scheme for positive feedback gain. Some literature derived the design criteria for positive feedback gain [35], [36]; however,

under constant power control (see Fig. 3(a)) they did not consider the weakening effect of the power PI regulators on the positive feedback, for PI regulators can suppress the interference in their control loops [37]. This is why an islanding detection is more difficult under constant power control than under constant current control [33]. In other words, these design criteria are not reliable. Additionally, for positive feedback gain, [35] and [36] only gave the minimum, while [28] indicated that it should not be too large. Hence, in reality, whether under constant power control or under constant current control, the positive feedback gain can only be obtained by trial and error. If one of the other parameters of the DG unit changes, the positive feedback gain may need to be updated through trial and error again. This is very inconvenient in the field environment for both users and service personnel, because islanding detection tests require some special equipment that is generally not equipped in the field environment.

b) The SFS method is no longer practicable under non-UPF control, which has been analyzed in detail in [7].

c) There is coupling between active current and reactive current control due to the inverse Givens transformation on the reference currents, i.e., i_{dref} and i_{qref} to $i_d^*$and i_q^* in Fig. 3, which may damage the current control performance.

d) Under constant current control, both the active current i_d and reactive current i_q have static errors due to the aforementioned coupling. From Fig. 3(b) it can be seen that the actual current i_d and i_q track i_d^* and i_q^*, rather than i_{dref} and i_{qref} that should have been tracked. When the frequency error (including fluctuation and measurement error of the frequency) is considered, i_{dref} and i_{qref} may be not equal to i_d^* and i_q^*. In other words, the inverter did not realize constant current under constant current control.

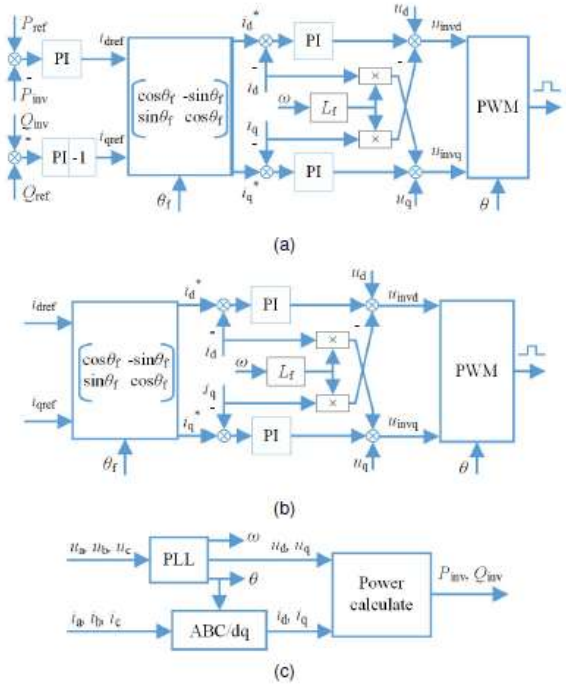

Fig. 3. Block diagrams of SFS method. (a) Constant power control. (b) Constant current control. (c) Acquisition of the related parameters

Moreover, in applications of wind turbine and solar generation, to achieve a high efficiency, a maximum power point tracking function is generally applied, which does not want the active current to be perturbed.

B. RCP Method and Its Problems

Under grid-voltage-oriented control, (7) is true. By substituting (7) into (3), (8) can be derived.

$$\begin{cases} P_{\text{inv}} = 3u_{\text{d}}i_{\text{d}}/2 \\ Q_{\text{inv}} = -3u_{\text{d}}i_{\text{q}}/2 \end{cases} \tag{7}$$

$$f_{\text{act}} = f_0(\sqrt{4Q_{\text{f}}^2 i_{\text{d}}^2 + i_{\text{q}}^2} + i_{\text{q}})/(2Q_{\text{f}}i_{\text{d}}) \tag{8}$$

Equation (8) means that a perturbation to i_q can also lead to a deviation of f_{act}. Consequently, the RCP method comes into being, which has been proposed in [4] and [5] and is an improvement on the SFS method. Specifically, the reformation is shown in Fig. 4. According to [4] and [5], the basic form of the reactive current perturbation is

$$i_{\text{per}}(f) = k_{\text{RCP}}(f - f_{\text{g}}) \tag{9}$$

where k_{RCP} is a positive feedback gain.

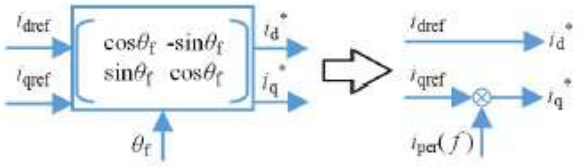

Fig. 4. Reformation of RCP method to SFS method

However, the RCP method has not overcome all the problems with the SFS method. There are still the two problems below.

a) The first problem with the SFS method shown in subsection II-A2 still exists.

b) There is still a static error with the reactive current under constant current control, for i_{qref} may be not equal to i_q^*.

Throughout the problems with the above two representative methods, the first problem of the two methods requires finding a reliable and convenient parameter selection scheme, whereas the other problems are caused by the principle of the two methods and thus there is no available remedy other than a fundamental improvement. We will address these problems in the next section.

III. An Improved Islanding Detection Method and a Reliable and Convenient Parameter Selection Scheme

A. Improved Method

According to the analysis in section II, the root cause of the current static errors is that the reference currents are perturbed. From this, we move the reactive current perturbation into the current loop, which is an important reformation to the RCP method, as shown in Fig. 5(a). The control block diagrams are shown in Figs. 5(b) and 5(c). $D_{i\_per}(f)$ is set to

$$D_{\text{i\_per}}(f) = k_{\text{pg}}(f - f_{\text{g}}) \tag{10}$$

where k_{pg} is a positive feedback gain. $D_{i\_per}(f)$ is actually a perturbation to the rate of change of reactive current, for the output of the reactive current PI regulator represents $L_f(di_q/dt)$ and L_f is a constant.

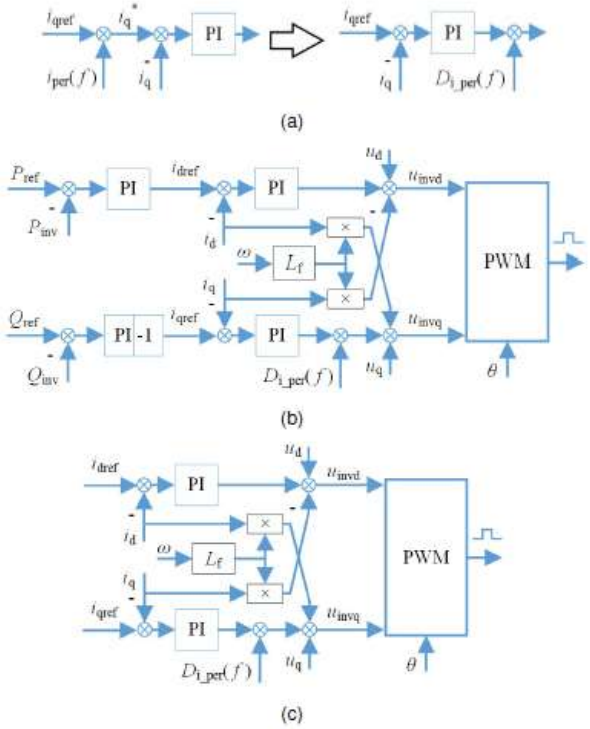

Fig. 5. A new perturbation and block diagrams of the improved method. (a) Reformation of the improved method to RCP method. (b) Constant power control. (c) Constant current control

In the improved method, i_d and i_q track i_{dref} and i_{qref} , respectively. Accordingly, in theory, there will not be any current static error. On the other hand, since a PI regulator can suppress the interference, especially the constant component (0 Hz) thereof, in its control loop, the improved method will be immune to the constant error of frequency. Besides that, the improved method inherits all the advantages of the RCP method.

B. Reliable and Convenient Parameter selection Scheme

As the perturbation from the improved method is in the current loop and does not affect the reference current, the positive feedback gain cannot be selected on the basis of the design criteria in [35], [36] any longer. In view of this, and in order to take into account the weakening effect of PI regulators on positive feedback, a new parameter selection scheme will be proposed in this subsection. This scheme is based on the idea that the perturbation $D_{i\_per}(f)$ should make the inverter system stable in grid-connected conditions and unstable in island conditions.

1) Constant Current Control in A Grid-Connected Condition: A system block diagram can be derived from Fig. 5(c), as shown in Fig. 6(a) [32]. Thereupon, the small signal model based on the perturbation can be derived from Fig. 6(a), as shown in Fig. 6(b).

From Fig. 6 it can be seen that the small signal model and the original system (i.e., Fig. 6(a) without the perturbation) have the same open-loop transfer function, which means that they possess the same stability according to the Nyquist stability criterion. In other words, the small signal model is stable since the original system must be stable, and thus the system represented by Fig. 6(a) is always stable.

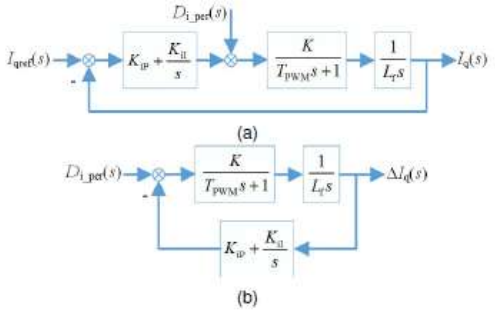

Fig. 6. System block diagram under constant current control and a grid-connected condition. (a) Block diagram with a perturbation. (b) Small signal model based on the perturbation.

2) *Constant Current Control in an Island Condition*: With regard to islanding detection, only the scenarios with small voltage and frequency variations in an island condition, i.e., close to power matching, are studied, for such islands cannot be detected by relay protection. Due to the small variations in voltage and frequency, in an island condition the block diagram is similar to Fig. 6(a) except that $D_{i\_per}(s)$ is already associated with $I_q(s)$, which will be shown later. To be able to analyze in the s-domain, (8) must be linearized. In order to simplify the analysis, i_d can be seen as a constant I_{d0} considering that it is not perturbed intentionally, and the steady-state operating point of i_q is seen as I_{q0}. Thereupon, the linearization of (8) is

$$\begin{cases} \Delta f_{act} = k_{iq\_f}\Delta i_q \\ k_{iq\_f} = f_0(I_{q0}/\sqrt{4Q_f{}^2I_{d0}{}^2 + I_{q0}{}^2} + 1)/(2Q_fI_{d0}) \end{cases} \tag{11}$$

where Δf_{act} and Δi_q are the variations of f_{act} and i_q around the steady-state operating points, respectively.

According to the principle of PLL, between f_{act} and f there is the relationship shown in Fig. 7, where K_{pllP} and K_{pllI} are the parameters of PLL regulator; and $\Delta\omega_{act}$ and $\Delta\omega$ are the variations of actual and measured angular frequencies around the steady-state operating points, respectively [38].

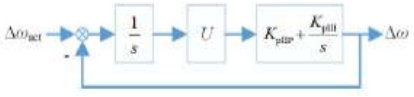

Fig. 7. Block diagram of PLL

Thus, the transfer function between Δf_{act} and Δf can be derived as follows.

$$W_{f\_pll}(s) = \frac{2\pi\Delta f}{2\pi\Delta f_{act}} = \frac{U(K_{pllP}s + K_{pllI})}{s^2 + UK_{pllP}s + UK_{pllI}} \tag{12}$$

As for the small signal model on (10), there is

$$\Delta D_{\text{i\_per}} = k_{\text{pg}} \Delta f \tag{13}$$

Accordingly, by combining (11)-(13), the small signal model for i_q is drawn in Fig. 8.

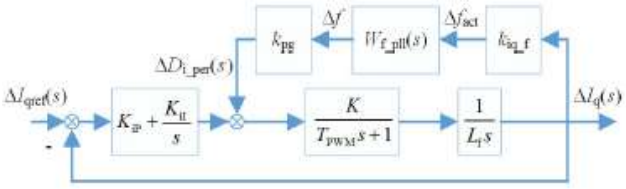

Fig. 8. Small signal model for the reactive current in an island condition

The transfer function of this small signal model $W_{iq\_isl}(s)$ is shown in (14).

According to automatic control theory, if a system is stable, the coefficients of its characteristic polynomial are of the same sign and not zero. Consequently, by observing the denominator of $W_{iq\_isl}(s)$, i.e., the characteristic polynomial, it can be derived that if the coefficient of s or s^2 is non-positive, the system represented by Fig. 8 must be unstable, from which the requirement for k_{pg} can be derived, as shown below.

$$k_{\text{pg}} \geq \frac{KK_{\text{iP}}K_{\text{pllP}}U + K_{\text{pllI}}L_{\text{f}}U + KK_{\text{iI}}}{KK_{\text{pllP}}Uk_{\text{iq\_f}}} \quad \text{or}$$

$$k_{\text{pg}} \geq \frac{K_{\text{iI}}K_{\text{pllP}} + K_{\text{iP}}K_{\text{pllI}}}{K_{\text{pllI}}k_{\text{iq\_f}}}$$

It should be noted that in the case of near-power matching, I_{d0} must be a positive value since it is close to the load active current. Thus k_{iq_f} is also a positive value according to (11), by which the above inequalities are obtained. In order to mitigate the amplification effect on the frequency error, theoretically, k_{pg} should take the smaller one of the boundary values of the two inequalities above. However, the small signal model shown in Fig. 8 is based on some approximations, and thus, to obtain a certain instability margin, k_{pg} should be larger than the smaller boundary value. Accordingly, a compromise that takes the average of these two boundary values is adopted. And in order to facilitate practical applications, k_{iq_f} is based on the most common scenario, i.e., unity power factor (UPF) control, by which there is the equation below from (11).

$$k_{\text{iq\_f}} = f_0/(2Q_{\text{f}}I_{\text{d0}})$$

Thereupon, under constant current control k_{pg} is set to

$$k_{\text{pg}} = \frac{Q_{\text{f}}I_{\text{nM}}[U_{\text{nM}}(KK_{\text{iI}}K_{\text{pllP}}{}^2 + 2KK_{\text{iP}}K_{\text{pllP}}K_{\text{pllI}} + L_{\text{f}}K_{\text{pllI}}{}^2) + KK_{\text{iI}}K_{\text{pllI}}]}{U_{\text{nM}}KK_{\text{pllP}}K_{\text{pllI}}f_{\text{g}}} \tag{15}$$

where U_{nM} is the amplitude of the rated voltage of the inverter, and substitutes for U due to the fact that the voltage is not perturbed intentionally by frequency shift methods and can be always seen as the rated voltage; I_{nM} is the amplitude of the rated current of the inverter (i.e., the maximum of I_{d0}), and substitutes for I_{d0} in order to keep the k_{pg} large enough in all situations; f_g substitutes for f_0 considering that under UPF control and power matching conditions f_0 is equal to f_g; Q_f can be set to the value specified in some standards, e.g., 1 in [31]; and K can be expressed as

$$K = U_{\text{BASE}}/I_{\text{BASE}}$$

where U_{BASE} and I_{BASE} are the base values to the voltage and current per-unit value, respectively.

3) Constant Power Control in a Grid-Connected Condition: Frequency shift methods are only aimed at shifting frequency. Thus, u_d can be seen as U_{nM}, i.e., a constant. According to (7), the Laplace transformation of Q_{inv} is

$$Q_{\text{inv}}(s) = -3U_{\text{nM}}I_{\text{q}}(s)/2$$

Thus, the system block diagram can be drawn in Fig. 9(a), where $W_{iq\ grid}(s)$ represents the block diagram in Fig. 6(a). The small signal model based on the perturbation can be obtained from Fig. 9(a), as shown in Fig. 9(b).

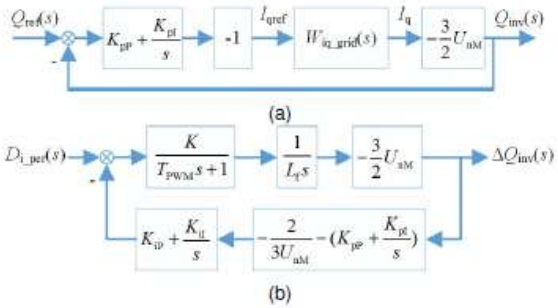

Fig. 9. System block diagram under constant power control and a grid connected condition. (a) Block diagram with a perturbation. (b) Small signal model based on the perturbation.

In the same way as subsection III-B1, it is found that this small signal model and the original system have the same characteristic polynomial. Consequently, the system represented by Fig. 9(a) must be stable.

4) Constant Power Control in an Island Condition: The small signal model is shown in Fig. 10 where $W_{iq\_isl}(s)$ represents the block diagram in Fig. 8.

By means of (14), the system transfer function of this small signal model $W_{Q\_isl}(s)$ can be obtained, as shown in (16). Accordingly, by following the approach in subsection III-B2, under constant power control k_{pg} is set as (17) to make the system unstable.

$$W_{\mathrm{iq\_isl}}(s)=\frac{K(K_{\mathrm{iP}}s+K_{\mathrm{iI}})(s^2+K_{\mathrm{pllP}}Us+K_{\mathrm{pllI}}U)}{\begin{array}{l}L_{\mathrm{f}}T_{\mathrm{pwm}}s^5+L_{\mathrm{f}}(K_{\mathrm{pllP}}T_{\mathrm{pwm}}U+1)s^4+(K_{\mathrm{pllI}}L_{\mathrm{f}}T_{\mathrm{pwm}}U+K_{\mathrm{pllP}}L_{\mathrm{f}}U+KK_{\mathrm{iP}})s^3+\\(KK_{\mathrm{iP}}K_{\mathrm{pllP}}U+K_{\mathrm{pllI}}L_{\mathrm{f}}U+KK_{\mathrm{iI}}-KK_{\mathrm{pllP}}Uk_{\mathrm{iq\_f}}k_{\mathrm{pg}})s^2+\\U(KK_{\mathrm{iI}}K_{\mathrm{pllP}}+KK_{\mathrm{iP}}K_{\mathrm{pllI}}-KK_{\mathrm{pllI}}k_{\mathrm{iq\_f}}k_{\mathrm{pg}})s+KK_{\mathrm{iI}}K_{\mathrm{pllI}}U\end{array}} \tag{14}$$

$$W_{\mathrm{Q\_isl}}(s)=\frac{\begin{array}{l}3U_{\mathrm{nM}}K(K_{\mathrm{pP}}s+K_{\mathrm{pI}})(K_{\mathrm{iP}}s+K_{\mathrm{iI}})(s^2+K_{\mathrm{pllP}}Us+K_{\mathrm{pllI}}U)\end{array}}{\begin{array}{l}2L_{\mathrm{f}}T_{\mathrm{pwm}}s^6+2L_{\mathrm{f}}(K_{\mathrm{pllP}}T_{\mathrm{pwm}}U+1)s^5+(2K_{\mathrm{pllI}}L_{\mathrm{f}}T_{\mathrm{pwm}}U+3KK_{\mathrm{iP}}K_{\mathrm{pP}}U_{\mathrm{nM}}+2K_{\mathrm{pllP}}L_{\mathrm{f}}U+\\2KK_{\mathrm{iP}})s^4+(3KK_{\mathrm{iP}}K_{\mathrm{pP}}K_{\mathrm{pllP}}UU_{\mathrm{nM}}+3KK_{\mathrm{iI}}K_{\mathrm{pP}}U_{\mathrm{nM}}+3KK_{\mathrm{iP}}K_{\mathrm{pI}}U_{\mathrm{nM}}+2KK_{\mathrm{iP}}K_{\mathrm{pllP}}U+\\2K_{\mathrm{pllI}}L_{\mathrm{f}}U+2KK_{\mathrm{iI}}-2KK_{\mathrm{pllP}}Uk_{\mathrm{iq\_f}}k_{\mathrm{pg}})s^3+K(3K_{\mathrm{iI}}K_{\mathrm{pP}}K_{\mathrm{pllP}}UU_{\mathrm{nM}}+3K_{\mathrm{iP}}K_{\mathrm{pI}}K_{\mathrm{pllP}}UU_{\mathrm{nM}}+\\3K_{\mathrm{iP}}K_{\mathrm{pP}}K_{\mathrm{pllI}}UU_{\mathrm{nM}}+3K_{\mathrm{iI}}K_{\mathrm{pI}}U_{\mathrm{nM}}+2K_{\mathrm{iI}}K_{\mathrm{pllP}}U+2K_{\mathrm{iP}}K_{\mathrm{pllI}}U-2K_{\mathrm{pllI}}Uk_{\mathrm{iq\_f}}k_{\mathrm{pg}})s^2+\\UK(3K_{\mathrm{iI}}K_{\mathrm{pI}}K_{\mathrm{pllP}}U_{\mathrm{nM}}+3K_{\mathrm{iI}}K_{\mathrm{pP}}K_{\mathrm{pllI}}U_{\mathrm{nM}}+3K_{\mathrm{iP}}K_{\mathrm{pI}}K_{\mathrm{pllI}}U_{\mathrm{nM}}+2K_{\mathrm{iI}}K_{\mathrm{pllI}})s+\\3KK_{\mathrm{iI}}K_{\mathrm{pI}}K_{\mathrm{pllI}}UU_{\mathrm{nM}}\end{array}} \tag{16}$$

$$k_{\mathrm{pg}}=\frac{\begin{array}{l}Q_{\mathrm{f}}I_{\mathrm{nM}}[3{U_{\mathrm{nM}}}^2K(K_{\mathrm{iI}}K_{\mathrm{pP}}{K_{\mathrm{pllP}}}^2+K_{\mathrm{iP}}K_{\mathrm{pI}}{K_{\mathrm{pllP}}}^2+2K_{\mathrm{iP}}K_{\mathrm{pP}}K_{\mathrm{pllP}}K_{\mathrm{pllI}})+U_{\mathrm{nM}}(3KK_{\mathrm{iI}}K_{\mathrm{pI}}K_{\mathrm{pllP}}\\+3KK_{\mathrm{iI}}K_{\mathrm{pP}}K_{\mathrm{pllI}}+2KK_{\mathrm{iI}}{K_{\mathrm{pllP}}}^2+3KK_{\mathrm{iP}}K_{\mathrm{pI}}K_{\mathrm{pllI}}+4KK_{\mathrm{iP}}K_{\mathrm{pllP}}K_{\mathrm{pllI}}+2L_{\mathrm{f}}{K_{\mathrm{pllI}}}^2)+2KK_{\mathrm{iI}}K_{\mathrm{pllI}}]\end{array}}{2U_{\mathrm{nM}}KK_{\mathrm{pllP}}K_{\mathrm{pllI}}f_{\mathrm{g}}} \tag{17}$$

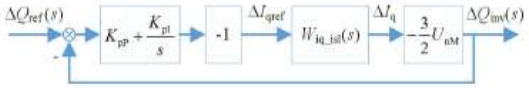

Fig. 10. Small signal model for the reactive power in an island condition

As mentioned above, the parameter selection scheme finally comes down to two algebraic expressions, i.e., (15) and (17), which means that the obtainment of k_{pg} only needs algebraic computation. Since all the PI parameters are involved in (15) and (17), the effect of PI regulators on positive feedback is considered. Thus the parameter selection scheme is reliable.

The PI parameters, e.g., K_{iP}, K_{pllP}, ... , can be tuned as in the regular control algorithm where there is no islanding detection method, for in grid-connected conditions the improved method only causes a small perturbation to the reactive current control. Since the parameters in (15) and (17) are either determined (e.g., Q_f , f_g, I_{nM}, L_f , K, etc.), or have been tuned in advance (e.g., K_{iP}, K_{pllP}, etc.), the parameter selection scheme is convenient enough to be implemented on a host computer, which reduces the computational burden of the microcontroller unit in which the control algorithm runs.

From (15) and (17) it can be seen that k_{pg} can be updated along with the variations of the parameters of inverters, filters and loads. Thus, the improved method (adopting the proposed parameter selection scheme) will not be affected by the variations of these parameters and will have a good environmental suitability. Furthermore, SFS and RCP methods are to lead to a power mismatch to achieve a frequency deviation, whereas the improved method is aimed at causing a system instability, by which frequency deviation is only one of the results. Since SFS and RCP methods do not pursue a system nstability, the frequencies may tend to stabilize before passing the limit, which is the direct reason for the NDZ. Therefore, for the improved method, there is theoretically no NDZ due to the system instability after island events.

In summary, the improved method eliminates the source of the current static error, and the parameter selection scheme yields a specific value for the positive feedback gain and needs no trial and error. Accordingly, the mentioned problems with the existing frequency shift methods are overcome. Table I demonstrates a comprehensive comparison between SFS, RCP and the improved methods.

TABLE I
Comparison between Three Islanding Detection Methods

	SFS	RCP	Improved Method
Is there a reliable and convenient parameter selection scheme?	No	No	Yes
Is it practicable under non-UPF control?	No	Yes	Yes
Are active current and reactive current control decoupled from each other?	No	Yes	Yes
Can the active current be controlled without a static error?	No	Yes	Yes
Can the reactive current be controlled without a static error?	No	No	Yes

IV. Simulation

The simulation platform is based on Matlab/Simulink, as shown in Fig. 11, where there is a 30 kW three-phase inverter equipped with an LCL filter and a 380 V/220 V grid- connected transformer.

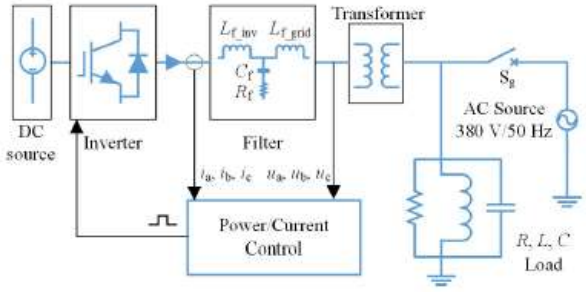

Fig. 11. Simulation platform

TABLE II
Simulation Parameters of the Inverter

K_{pp}	K_{PI}	K_{iP}	K_{iI}	K_{PIIP}	K_{PIII}	K	L_{f_inv}(mH)	L_{f_grid}(mH)	Cf (μF)	Rf (Ω)
									Y-connection	
0.002	0.08	10.5	500	1	17.8	1	0.4	0.1	90	0.3

Through parameter tuning, the parameters of the inverter are set to the values shown in Table II. Since the larger the Q_f , the harder the islanding detection is, the load is designed to be with a Q_f of 2.5 rather than 1 [39].

A. Current Errors Validation

The simulations in this subsection are based on constant current control. According to (6), (9), (10) and (15), the parameters of the three mentioned methods are set as

$$\theta_f = [cf_0 + 0.2(f-50)]\pi/2,\ cf_0 = 0 \text{ or } 0.01$$
$$i_{per}(f) = 28(f-50)$$
$$D_{i\_per}(f) = 291(f-50)$$

A frequency error that contains a positive constant component and an alternating component is assumed and is set to

$$f_{err} = [0.02 + 0.035\sin(20\pi t)]\ \text{Hz}$$

Thereupon, f (i.e., f_g+f_{err}) can be illustrated in Fig. 12, and the simulation results are shown in Fig. 13.

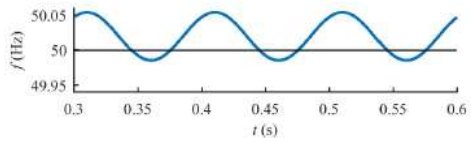

Fig. 12. Frequency with a hybrid error

In Fig. 13, although there are reactive current static errors with all the three methods, the static errors resulting from the SFS method are evidently larger, about 0:7A + 1:3A peak (i.e., the constant portion 0:7A + the alternating portion with an amplitude of 1:3A) and 2:4A + 1:3A peak for the conditions with $cf_0 = 0$ and $cf_0 = 0{:}01$, respectively, which also indicates that a non-zero cf_0 will intensify such errors in some cases. The reactive current static errors with the RCP and the improved methods are about 0:5A+1A peak and 0:9A peak, respectively. Although the errors with both the methods are smaller, only the improved method eliminates the constant portion of the error, which means that from an average point of view the reactive current has no error.

B. Evaluation of the Improved Method and the Parameter Selection Scheme Based on IEEE Std 1547.1-2005

A normal frequency range depends on the local grid codes and is set to [48 Hz, 50.5 Hz] in this paper. According to (10) and (17), under constant power control $D_{i\_per}(f)$ is set to

$$D_{i\_per}(f) = 545(f-50)$$

An island is formed by disconnecting the S_g in Fig. 11 at 0.6 s. The simulation results are shown in Fig. 14. Once the frequency passes the limit, i.e., above 50.5 Hz or below 48 Hz, a trip signal will be produced. The cases with longer trip time (i.e., the time between an island event and the corresponding trip signal) are shown in Table III, where P and P_{qL} are the load active power and inductive reactive power, respectively. As for the cases with shorter trip time, where P = 100%, P_{qL} = 95%-98% and P_{qL} = 105%-102%, their simulation results are shown on the left side of Fig. 14.

TABLE III
Test Cases Based on IEEE Std 1547.1-2005

Cases	P (%)	P_qL (%)	R (Ω)	L (Mh)	C (mF)	Q_f
1	100	100	4.84	6.124	1.634	2.5
2	100	99	4.84	6.186	1.634	2.49
3	100	101	4.84	6.063	1.634	2.51
4	66	100	7.26	9.138	1.084	2.5
5	66	99	7.26	9.23	1.084	2.49
6	66	101	7.26	9.048	1.084	2.51
7	33	100	14.52	18.03	0.5344	2.5
8	33	99	14.52	18.21	0.5344	2.49
9	33	101	14.52	17.85	0.5344	2.51

According to Fig. 14, after the island events occurring at 0.6 s, the frequencies in all cases begin to be destabilized and finally deviate from the normal range. The longest trip time is from case 1, about 0.1 s, which infers that islanding detection will be the most difficult under the condition of case 1. When P is a constant, the trip time decreases as P_{qL} moves away from 100% (i.e., completely power-matching); when P_{qL} is a constant (e.g., cases 1, 4, 7), the trip time decreases as P moves down from 100%. In IEEE Std 1547.1- 2005, P actually also represents the ratio of the inverter power to its rated power. Therefore, these results indicate that for the improved method, both a higher power-matching degree and a larger inverter power will bring about a more difficult islanding detection. However, Fig. 14 shows that every island can be detected within much less than 2 s, which entirely satisfies IEEE Std 1547.1-2005 and therefore demonstrates the effectiveness of both the improved method and the parameter selection scheme.

V. Experiment

The experimental plant is the same as that shown in Fig. 11 except that the rated power of the inverter is 3 kW, the filter is a single-L and the transformer ratio is 380 V/190 V. A DSP (TI F28335) is used as the control core. There is no extra hardware cost for the improved method. The related parameters are shown in Table IV.

TABLE IV
Experimental Parameters of the Inverter

K_{PP}	K_{PI}	K_{iP}	K_{iI}	K_{KIIP}	K_{PIII}	K	L_f(mH)
0.5	20	1	50	1400	5000	25.3	5

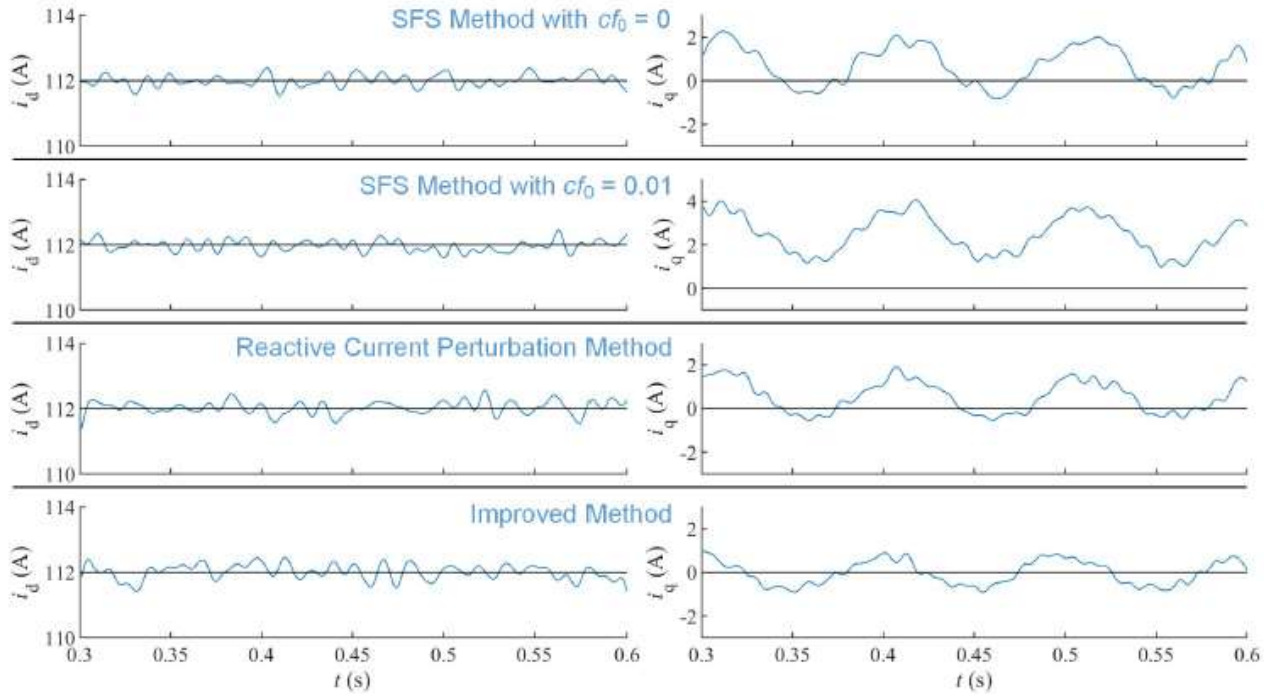

Fig. 13. i_d and i_q based on a hybrid frequency error and UPF control (i_{dref} = 112A (i.e., amplitude of the rated current) and i_{qref} = 0)

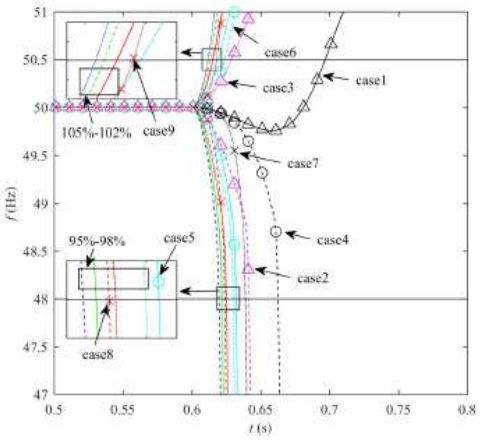

Fig. 14. Frequencies before and after the island events

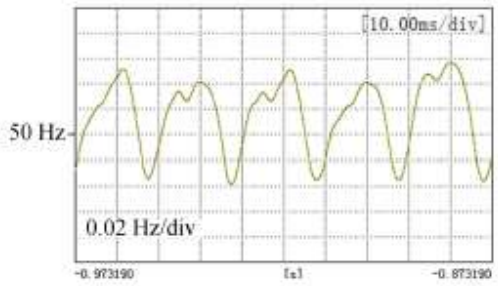

Fig. 15. Frequencies before and after the island events

A. Current Errors Validation

Under constant current control, the perturbations of the three mentioned methods are set as follows.

$$\theta_f = [cf_0 + 0.2(f-50)]\pi/2,\ cf_0 = 0 \text{ or } 0.01$$
$$i_{per}(f) = 0.494(f-50)$$
$$D_{i\_per}(f) = 0.494(f-50)$$

As regards the frequency error, there has been a little fluctuation in the measured frequency, and besides that, a constant error of -0.02 Hz is artificially added to the measured frequency, which only affects the perturbations. The final frequency waveform is shown in Fig. 15. and the experimental results are shown in Fig. 16.

In Fig. 16, for the SFS method, although the reactive current static errors are smaller, the active currents have obvious static errors, about 0:2A peak and 0:2A + 0:2A peak for the conditions with cf_0 = 0 and cf_0 = 0:01, respectively, which are undesirable in generation. There are still only reactive current static errors with the RCP and the improved methods, about 0:3A + 0:5A peak and 0:5A peak, respectively. Thus, in contrast, still only by applying the improved method, there is no error with the active current and only alternating error with the reactive current.

B. Performance of the Improved Method and the Parameter Selection Scheme

From the previous simulation results, islanding detection is more difficult in the cases of power matching (i.e., with longer trip time). Thus, such three cases whose power level is the same as that of the cases 1, 4 and 7 shown in Table III are

tested. $D_{i\_per}(f)$ is set as follows according to (10) and (17).

$$D_{i\_per}(f) = 0.686\,(f - 50)$$

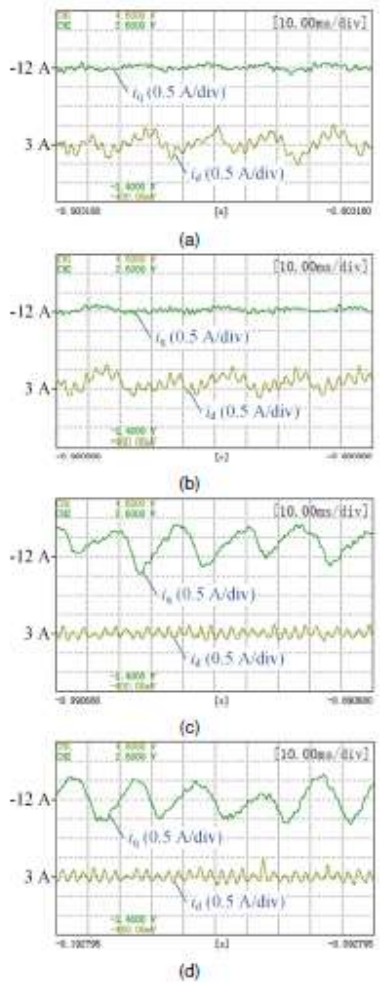

Fig. 16. Actual active and reactive currents (i_{dref} = 3A and i_{qref} = -12A). (a) SFS method with cf_0 =0. (b) SFS method with cf_0 = 0.01. (c) RCP method. (d) Improved method.

The experimental results are shown in Fig. 17. In order to clearly show the moment when the frequency passes the limit, the displayable frequency range is set to [47.8 Hz, 52.2 Hz] for the oscilloscope, which both contains the normal frequency range and is not too wide.

From the experimental results in Fig. 17, we can see that all the frequencies rise sharply and pass the upper limit (i.e., 50.5 Hz) in 0.01 s after the island events, by which the islands are detected quickly and then the inverter halts itself.

In conclusion, the experimental results verify the performance of the improved method, and show that the proposed parameter selection scheme is reliable and, since there is no trial and error, it is also convenient.

VI. Conclusion

A solution aimed at parameter selection and current static error issues with frequency shift islanding detection methods is proposed in this paper. It includes an improved method and a reliable and convenient parameter selection scheme for positive feedback gain. On the one hand, the improved method removes the source of current errors, by which there is no error with the active current, and the reactive current also has no error from an average point of view. On the other hand, the parameter selection scheme which is based on system stability analyses considers the weakening effect of the PI regulator on the positive feedback and does not require trial and error. Thus, the work in this paper makes such islanding detection methods more applicable in practice, especially in field environments.

Although the improved method is suggested, the users that still plan to use the present frequency shift methods can follow the idea in this paper to derive the applicable parameter selection scheme in their methods.

References

[1] M. Khodaparastan, H. Vahedi, F. Khazaeli, and H. Oraee, "A novel hybrid islanding detection method for inverter-based dgs using sfs and rocof," *IEEE Transactions on Power Delivery*, vol.32, no.5, pp.2162-2170, Oct.2017.

[2] S. Akhlaghi, A. Akhlaghi, and A. A. Ghadimi, "Performance analysis of the slip mode frequency shift islanding detection method under different inverter interface control strategies," in *2016 IEEE Power and Energy Conference at Illinois (PECI)*, pp. 1–7. Urbana, IL, USA: IEEE, Feb. 2016.

[3] G. Hernandez-Gonzalez and R. Iravani, "Current injection for active islanding detection of electronically-interfaced distributed resources," *IEEE Transactions on Power Delivery*, vol.21, no.3, pp.1698-1705, Jul. 2006.

[4] J.-H. Chiu, Y.-R. Chang, F.-J. Lin, Y.-S. Huang, and K.-H. Tan, "Active islanding detection method using d-axis disturbance signal injection with intelligent control," *IET Generation, Transmission & Distribution*, vol.7, no.5, pp.537-550, 2013.

[5] Y. Jiao, Q. Song, and W. Liu, "Decoupled instantaneous current control and islanding detection strategy for a single-phase photovoltaic generation system," in *IECON 2010 - 36th Annual Conference on IEEE Industrial Electronics Society*, pp.3210-3215. Glendale, AZ, USA: IEEE, Nov.2010.

[6] J. B. Jeong, H. J. Kim, K. S. Ahn, and C. H. Kang, "A novel method for anti-islanding using reactive power," in *Twenty-Seventh International Telecommunications Conference, INTELEC'05*., pp. 101-106. Berlin, Germany: IEEE, Sep. 2005.

[7] M. Liu, W. Zhao, S. Huang, Q. Wang, and K. Shi, "Problems in the classic frequency shift islanding detection methods applied to energy storage converters and a coping strategy," *IEEE Transactions on Energy Conversion*, vol.33, no.2, pp.496-505, Jun, 2018.

[8] J. Munoz-Cruzado-Alba, J. Villegas-Nunez, J. A. Vite-Frias, J. M. Carrasco-Solis, and E. Galvan-Diez, " New low-distortion q-f droop plus correlation anti-islanding detection method for power converters in distributed generation systems," *IEEE Transactions on Industrial Electronics*, vol.62, no.8, pp.5072-5081, Aug. 2015.

[9] Y. Jin, Q. Song, and W. Liu, "Anti-islanding protection for distributed generation systems based on reactive power drift," pp.3970-3975.IEEE, Nov.2009.

[10] B. H. Kim and S. K. Sul, "Comparison of non-detection zone of frequency drift anti-islanding with closed-loop power controlled distributed generators," in *Future Energy Electronics Conference*, pp.1-5, Taipei, Taiwan, Nov. 2015.

[11] H. Vahedi and M. Karrari, "Adaptive fuzzy sandia frequency-shift method for islanding protection of inverter-based distributed generation," *IEEE Transactions on Power Delivery*, vol.28, no.1, pp.84-92, Jan. 2013.

Fig. 17. Frequencies before and after the island events. The power level of (a) – (c) is the same as that of the cases 1, 4 and 7 shown in Table III, respectively, fmax = 52.2 Hz is the maximum value that can be displayed on the oscilloscope

[12] M. Al Hosani, Z. Qu, and H. H. Zeineldin, "Scheduled perturbation to reduce nondetection zone for low gain sandia frequency shift method," *IEEE Transactions on Smart Grid*, vol.6, no.6, pp. 3095-3103, Nov. 2015.

[13] S. Akhlaghi, M. Sarailoo, A. Akhlaghi, and A. A. Ghadimi, "A novel hybrid approach using sms and recof for islanding detection of inverterbased dgs," in *2017 IEEE Power and Energy conference at lllinois (PECI)*, PP.1-7, Champaign, IL, USA, Feb, 2017.

[14] H. Vahedi, M. Karrari, and G. B. Gharehpetian, "Accurate sfs parameter design criterion for inverter-based distributed generation," *IEEE Transactions on Power Delivery*, vol.31, no.3, pp.1050-1059, Jun. 2016.

[15] D. Voglitsis, N. Papanikolaou, and A. C. Kyritsis, "Incorporation of harmonic injection in an interleaved flyback inverter for the implementation of an active anti-islanding technique," *IEEE Transactions on Power Electronics*, vol.32, no.11, pp.8526-8543, Nov. 2017.

[16] W. Cai, B. Liu, S. Duan, and C. Zou, "An islanding detection method based on dual-frequency harmonic current injection under grid impedance unbalanced condition," *IEEE Transactions on Industrial Informatics*, vol. 9, no.2, pp.1178-1187, May.2013.

[17] M. Liu, W. Zhao, Q. Wang, S. Huang, and K. Shi, "An irregular current injection islanding detection method based on an improved impedance measurement scheme," *Energies*, vol.11, no.9, pp2474, 2018.

[18] N. Liu, C. Diduch, L. Chang, and J. Su, "A reference impedance based passive islanding detection method for inverter-based distributed generation system," *IEE Journal of Emerging and Selected Topics in Power Electronics*, vol.3, no.4, pp.1205-1217, Dec.2015.

[19] S. A. Saleh, A. S. Aljankawey, R. Meng, J. Meng, L. Chang, and C. P. Diduch, "Apparent power-based anti-islanding protection for distributed cogeneration systems," *IEEE Transactions on Industry Applications*, vol.52, no.1, pp. 83-98, January/February 2016.

[20] S. Agrawal, S. Patra, S. R. Mohanty, V. Agarwal, and M. Basu, "Use of matrix-pencil method for efficient islanding detection in static dg and a parallel comparison with dwt method," *IEEE Transactions on Industrial Electronics*, vol.66, no.11, pp.8937-8946, Nov.2019.

[21] F. Yang, N. Xia, and Q.-L. Han, "Event-based networked islanding detection for distributed solar pv generation systems," *IEEE Trainsactions on Industrial Informatics,* vol. 13, no.1, pp.322-329, Feb. 2017.

[22] R. Nale, M. Biswal, and N. Kishor, "A transient component based approach for islanding detection in distributed generation," *IEEE Transactions on Sustainable Energy*, vol. 10, no.3, pp.1129-1138, Jul. 2019.

[23] D. M. Laverty, R. J. Best, and D. J. Morrow, "Loss-of-mains protection system by application of phasor measurement unit technology with experimentally assessed threshold settings," *IET Generation, Transmission & Distribution,* vol.9, no.2, pp.146-153, 2015.

[24] A. M. Mohamad and Y. A.-R. I. Mohamed, "Impedance-based analysis and stabilization of active dc distribution systems with positive feedback islanding detection schemes," *IEEE Transaction on Power Electronics*, vol.33, no.11, pp.9902-9922, Nov. 2018.

[25] C. N. Papadimitriou, V. A. Kleftakis, and N. D. Hatziargyriou, "A novel method for islanding detection in dc networks," *IEEE Transactions on Sustainable Energy,* vol. 8, no.1, pp.441-448, Jan 2017.

[26] D. Mlaki´c, H. R. Baghaee, and S. Nikolovski, "Gibbs phenomenon-based hybrid islanding detection strategy for vsc-based microgrids using frequency shift, thdu and rmsu," *IEEE Transactions on Smart Grid*, vol.10, no.5, pp.5479-5491, Sep. 2019.

[27] X. Chen, Y. Li, and P. Crossley, "A novel hybrid islanding detection method for grid-connected microgrids with multiple inverter-based distributed generators based on adaptive reactive power disturbance and passive criteria," *IEEE Transactions on Power Electronics*, vol.34, no.9, pp.9342-9356, Sep. 2019.

[28] W. Xiaoyu, W. Freitas, V. Dinavahi, and W. Xu, "Investigation of positive feedback anti-islanding control for multiple inverter-based distributed generators," *IEEE Transactions on Power Systems*, vol. 24, DOI 10.1109/TPWRS.2008.2007002, no. 2, pp. 785-795, May. 2009.

[29] M. E. Ropp, "Design issues for grid-connected photovoltaic systems," Ph.D. dissertation, Georgia Institute of Technology, Atlanta, 1998.

[30] G. Kern, R. Bonn, J. Ginn, and S. Gonzalez, "Results of sandia national laboratories grid-tied inverter testing," Sandia National Labs, Albuquerque, NM (United States), Albuquerque, Tech. Rep., 1998.

[31] IEEE 1547. 1-2005, *IEEE Standard Conformance Test Procedures for Equipment Interconnecting Distributed Resources with Electric Power Systems*. New Yprk: IEEE, 2005.

[32] E. Figueres, G. Garcer´a, J. Sandia, F. Gonzalez-Espin, and J. C. Rubio, "Sensitivity study of the dynamics of three-phase photovoltaic inverters with an lcl grid filter," *IEEE Transactions on Industrial Electronics*, vol. 56, no.3, pp.706-717, Mar. 2009.

[33] X. Wang, W. Freitas, W. Xu, and V. Dinavahi, "Impact of dg interface controls on the sandia frequency shift antiislanding method," *IEEE Transactions on Energy Conversion*, vol. 22, no. 3, pp.792-794, Sep. 2007.

[34] L. A. C. Lopes and H. Sun, "Performance assessment of active frequency drifting islanding detection methods," *IEEE Transactions on Energy Conversion*, vol. 21, no.1, pp.171-180, Mar. 2006.

[35] H. Sun, L. A. C. Lopes, and Z. Luo, "Analysis and comparison of islanding detection methods using a new load parameter space," in *30th Annual Conference of IEEE Industrial Electronics Society*, vol. 2, pp.1172-1177. Busan, South Korea: IEEE, Nov. 2004.

[36] H. H. Zeineldin and S. Kennedy, "Sandia frequency-shift parameter slection to eliminate nondetection zones," *IEEE Transactions on Power Delivery*, vol. 24, no.1, pp.486-487, Jan. 2009.

[37] H. Geng, D. Xu, B. Wu, and G. Yang, "Design and comparison of active frequency drifting islanding detection methods for dg systems with different interface controls," in *International Symposium on Power Electronics for Distributed Generation Systems*, pp.459-465. Hefei, China: IEEE, Jun. 2010.

[38] V. Kaura and V. Blasko, "Operation of a phase locked loop system under distorted utility conditions," *IEEE Transactions on Industry Applications*, vol. 33, no.1, pp.58-63, January/February 1997.

[39] M. Al Hosani, Z. Qu, and H. H. Zeineldin, "Development of dynamic estimators for islanding detection of inverter-based dg," *IEEE Transactions of Power Delivery,* vol. 30, no. 1, pp.428-436, Feb. 2015.